Spectrochimica Acta Part A: Molecular and Biomolecular Spectroscopy 139 (2015) 346–355

Contents lists available at ScienceDirect

Spectrochimica Acta Part A: Molecular and Biomolecular Spectroscopy

journal homepage: www.elsevier.com/locate/saa

Conformational and spectroscopic study of xanthogen ethyl formates, ROC(S)SC(O)OCH$_2$CH$_3$. Isolation of CH$_3$CH$_2$OC(O)SH

Luciana C. Juncal, Melina V. Cozzarín, Rosana M. Romano *

CEQUINOR (CONICET-UNLP), Departamento de Química, Facultad de Ciencias Exactas, Universidad Nacional de La Plata, 47 esq. 115, (1900) La Plata, Argentina

HIGHLIGHTS

- ROC(S)SC(O)OEt molecules present three groups of different conformers in equilibrium.
- The *syn–syn* conformers are stabilized in liquid phase by intermolecular interactions.
- The unknown CH$_3$CH$_2$OC(O)SH was isolated by Ar-matrix photolysis of CH$_3$OC(S)SC(O)OEt.

GRAPHICAL ABSTRACT

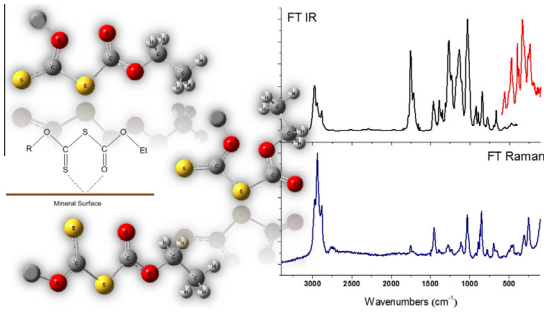

ARTICLE INFO

Article history:
Received 29 July 2014
Received in revised form 7 December 2014
Accepted 17 December 2014
Available online 30 December 2014

Keywords:
Conformations
Vibrational spectroscopy
Photochemistry

ABSTRACT

ROC(S)SC(O)OCH$_2$CH$_3$, with R = CH$_3$—, (CH$_3$)$_2$CH— and CH$_3$(CH$_2$)$_2$—, were obtained through the reaction between potassium xanthate salts, ROC(S)SK, and ethyl chloroformate, ClC(O)OCH$_2$CH$_3$. The liquid compounds were identified and characterized by ^{1}H and ^{13}C NMR and mass spectrometry. The conformations adopted by the molecules were studied by DFT methods. 6 conformers were theoretically predicted for R = CH$_3$— and (CH$_3$)$_2$CH—, while the conformational flexibility of the n-propyl substituent increases the total number of feasible rotamers to 21. For the three molecules, the conformers can be associated in 3 groups, being the most stable the **AS** forms – the C=S double bond *anti* (**A**) with respect to the C—S single bond and the S—C single bond *syn* (**S**) with respect to the C=O double bond – followed by **AA** and **SS** conformers. The vibrational spectra were interpreted in terms of the predicted conformational equilibrium, presenting the ν(C=O) spectral region signals corresponding to the three groups of conformers. A moderated pre-resonance Raman enhancement of the ν(C=S) vibrational mode of CH$_3$(CH$_2$)$_2$OC(S)SC(O)OCH$_2$CH$_3$ was detected, when the excitation radiation approaches the energy of a $n \rightarrow \pi^*$ electronic transition associated with the C=S chromophore. UV–visible spectra in different solvents were measured and interpreted in terms of TD-DFT calculations. The unknown molecule CH$_3$CH$_2$OC(O)SH was isolated by the UV–visible photolysis of CH$_3$OC(S)SC(O)OCH$_2$CH$_3$ isolated in Ar matrix, and also obtained as a side-product of the reaction between potassium xanthate salts, ROC(S)SK, and ethyl chloroformate, ClC(O)OCH$_2$CH$_3$.

Introduction

Xanthogen formates are compounds with the general formula R^{1}OC(S)SC(O)OR^2, with R^1 and R^2 alkyl or aryl groups. Their abilities as flotation collectors, particularly for metallic sulfides of Cu(II) and Zn(II), have been known since 1927 [1,2]. The advantage of the use of xanthogen formates instead of xanthate salts in mining and metallurgical processes is related with the stability of the former compounds in acidic media, while the salts usually need pH above 10 to avoid decomposition [3]. The collector properties of a series of different molecules having in common the isopropyl

* Corresponding author.
E-mail address: romano@quimica.unlp.edu.ar (R.M. Romano).

http://dx.doi.org/10.1016/j.saa.2014.12.086
1386-1425/

substituent, including not only a xanthogen formate and a xanthate salt but also a dixantogen, a dithiophosphate and a thiocarbamate, have been comparatively evaluated, concluding that the xanthogen formate is an excellent collector for copper sulfide [4].

The role of the substituents R^1 and R^2 in the collector ability of the xanthate salts and xanthogen molecules has been evaluated by Ackerman et al. [3], finding that for the xanthates the main effect of the alkylic group in the flotation process is the increment of the insolubility and hydrophobicity of the adsorbed species. On the other hand, they proposed a chelation mechanism for the interaction between the xanthogens and the metallic sulfides, occurring probably by both, the oxygen and the sulfur atoms of the carbonylic and thiocarbonylic groups, respectively. Although the chelate complex is unknown, the structure and conformations of the molecules, as well as the substituents R^1 and R^2, are expected to play an important role in the collector properties. A molecular conformation that allows the formation of a ring involving five atoms of the xanthogen, ···S═C—S—C═O···, and the mineral surface, should surely favor the chelation mechanisms.

The effect of the substituents consists mainly in an alteration of the electronic density over the interacting O and S atoms. Recently, a QSAR analysis of the selectivity of different xanthogen molecules in the flotation of chalcopyrite ($CuFeS_2$) was published [5]. Six theoretical descriptors were employed in this study, being the electronic density of the LUMO orbital one of the most important descriptors that influences the flotation selectivity. In a previous theoretical work, not only the energy and character of the LUMO orbital but also the characteristic of the HOMO orbital are proposed to explain the reactivity and consequent collector ability of different compounds [6,7].

Despite the interest in xanthogen compounds regarding their collector properties, as described above, no structural, conformational and spectroscopic studies were found in the literature. In this work the experimental and theoretical conformational, vibrational and electronic studies of three xanthogen ethyl formates, $ROC(S)SC(O)OCH_2CH_3$, with R = CH_3—, $(CH_3)_2CH$— and $CH_3(CH_2)_2$—, are presented. The compounds were synthesized following a reported procedure [8], and the identity and purity of the molecules were checked by ^1H and ^{13}C NMR and GC–MS. $CH_3CH_2OC(O)SH$ was detected as a side-product of the xanthogens synthesis. To the best of our knowledge, there is no previous report of this molecule in the literature. Only its salts were identified as a decomposition product during the flotation process [9]. The matrix-isolation photochemistry of the smallest molecule, $CH_3OC(S)SC(O)OCH_2CH_3$, was also investigated. The main photochannel conducts also to the formation of $CH_3CH_2OC(O)SH$.

Experimental

Materials

Reagents (ROH, with R = CH_3—, $(CH_3)_2CH$— and $CH_3(CH_2)_2$—, CS_2, KOH and $ClC(O)OCH_2CH_3$) were purchased reagent grade and used without further purification. Solvents ($CH_3CH_2OCH_2CH_3$, $CH_3C(O)CH_3$, CCl_4, $CHCl_3$, CH_3OH and CH_3CN) were dried using molecular sieves. Potassium xanthate salts, ROC(S)SK with R = CH_3—, $(CH_3)_2CH$— and $CH_3(CH_2)_2$—, were prepared and purified according to literature procedures from KOH, CS_2, and the corresponding alcohol, ROH [10].

Synthesis

Xanthogen ethyl formates, $ROC(S)SC(O)OCH_2CH_3$ with R = CH_3—, $(CH_3)_2CH$— and $CH_3(CH_2)_2$—, were prepared by the reaction of the corresponding potassium xanthate salts ROC(S)SK, and ethyl chloroformate, $ClC(O)OCH_2CH_3$. The reactants were mixed at 0 °C, and the reaction mixtures were stirring during 5 h, allowing reaching slowly ambient temperatures. Pure samples of $ROC(S)SC(O)OCH_2CH_3$ were isolated from reduced-pressure distillation after filtration of the solids formed during the reaction as yellow liquids, and subsequently purified by repeated trap-to-trap distillation in vacuum conditions. A more detailed description of the synthesis conditions is presented in the Supplementary material. The purity of the samples was controlled along the purification processes by GC–MS. As a side-product of the reactions $CH_3CH_2OC(O)SH$ was identified.

Gas chromatography–mass spectrometry

The GC–MS analysis was carried out on a Shimadzu QP-2010. Details are given in Table S1 of the Supplementary material. Figs. S1–S3 show the chromatograms obtained during the purification processes from CCl_4 solutions of approximately 200 ppm. In the conditions specified in Table S1, the elution times were 6.9, 8.5 and 9.6 min for methyl, isopropyl and n-propyl compounds, respectively, while the chromatographic peak assigned to $CH_3CH_2OC(O)SH$ was observed at 5.5 min.

NMR spectroscopy

The ^1H (200 MHz) and ^{13}C (50 MHz) NMR spectra of the samples were measured at 298 K on a Varian Mercury Plus 200 spectrometer. Each of the compounds was dissolved in $CDCl_3$ in a 5 mm NMR tube. Chemical shifts, δ, are given in ppm relative to TMS (δ = 0 ppm).

FTIR spectroscopy

The FTIR spectra were recorded on a Nexus Nicolet instrument equipped with either an MCTB or a DTGS detector (for the ranges 4000–400 cm^{-1} or 600–100 cm^{-1}, respectively) at room temperature and with a resolution of 4 cm^{-1}. The IR spectra of the neat liquids were measured between KBr, CsI and polyethylene windows, to cover the range between 4000 and 100 cm^{-1}.

Raman spectroscopy

The FTRaman spectra were measured in a Bruker IFS 66 FTRaman spectrometer, using a resolution of 4 cm^{-1}, in the region between 3500 and 100 cm^{-1}. The samples, placed in a sealed

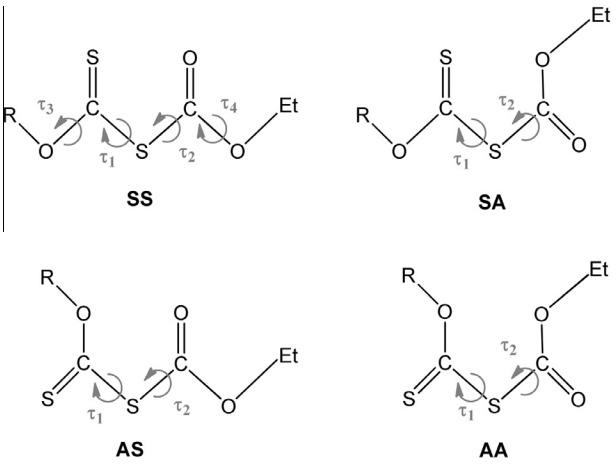

Scheme 1. Schematic representation of the *syn*(**S**) and *anti*(**A**) orientation in terms of the dihedral angles τ_1(S═C—S—C) and τ_2 (C—S—C═O) for ROC(S)SC(O)OEt molecules.

Table 1
Relative energies and populations of the most stable conformers of ROC(S)SC(O)OCH_2-CH_3, with R = CH_3 and $(CH_3)_2CH$—, calculated with the B3LYP/6-31 + G* approximation.

Conformer[a]	**AS**		**AA**		**SS**	
	AS-A	**AS**-G	**AA**-A	**AA**-G	**SS**-A	**SS**-G
$CH_3OC(S)SC(O)OCH_2CH_3$						
ΔE (kcal/mol)	0.00	0.47	1.42	1.75	1.40	1.82
% (298 K)[b]	48.2	35.1	6.0	5.4	3.3	2.1
	83.3		9.4		5.4	
$(CH_3)_2CHOC(S)SC(O)OCH_2CH_3$						
ΔE (kcal/mol)	0.00	0.48	1.79	1.92	1.68	2.17
% (298 K)[b]	51.9	37.4	3.4	2.3	2.7	2.2
	89.3		5.7		4.9	

[a] The first letter, **A** or **S**, refers to the *anti* or *syn* orientation of the C═S with respect to the C—S, the second letter corresponds to the orientation of the S—C with respect to the C═O, and the third one describes the two possible orientation of the ethyl terminal group, anti (A) or gauche (G).
[b] Calculated from $\Delta G°$ according to the Boltzmann law, with 2 multiplicity for the *gauche* forms.

2 mm glass capillary, were excited with a 1064 nm Nd-YAG laser. The resonance or pre-resonance Raman effect was investigated using an Horiba-Jobin-Yvon T64000 Raman spectrometer, with a confocal microscope and CCD detection, employing different excitation wavelength from Ar and Kr multiline lasers. The wavenumbers were calibrated with the 459 cm^{-1} band of CCl_4. CH_3CN was used as internal standard for the pre-resonant Raman study.

Matrix isolation and photochemistry

1 L vacuum flasks containing the vapor of each of the compounds were filled with ca. 500 Torr of Ar. The gas mixtures were deposited on a CsI window cooled to ca. 15 K by means of a Displex closed-cycle refrigerator (SHI-APD Cryogenics, model DE-202) using the pulse deposition technique [11,12]. The matrix-isolated FTIR spectra were recorded on a Nexus Nicolet instrument described previously. Following deposition and IR analysis of the resulting matrixes, the samples were exposed to broad-band UV–visible radiation ($200 \leqslant \lambda \leqslant 800$ nm) from a Spectra-Physics Hg–Xe arc lamp operating at 1000 W. The output from the lamp was limited by a water filter to absorb IR radiation and so minimize any heating effects. The IR spectra of the matrixes with 0.5 and 0.125 cm^{-1} resolution were then recorded at different times of irradiation in order to monitor closely any change in the spectra.

Table 2
Relative energies and populations of the most stable conformers of $CH_3(CH_2)_2$-$OC(S)SC(O)OCH_2CH_3$ calculated with the B3LYP/6-31+G* approximation.

Conformer[a]	ΔE (kcal/mol)	% (298 K)[b]
A-**AS**-A	0.19	29.9
G±-**AS**-A	0.00	27.2
A-**AS**-G±	0.72	13.6
G+-**AS**-G+	0.54	4.4
G+-**AS**-G−	0.55	4.8
G−-**AS**-G+	0.55	4.8
G−-**AS**-G−	0.54	4.4
A-**AA**-A	1.81	1.6
G±-**AA**-A	1.89	1.2
A-**AA**-G±	2.31	1.0
G+-**AA**-G+	2.39	0.4
G+-**AA**-G−	2.59	0.2
G−-**AA**-G+	2.59	0.2
G−-**AA**-G−	2.39	0.4
A-**SS**-A	1.72	1.0
G±-**SS**-A	1.73	2.5
A-**SS**-G	2.24	0.8
G+-**SS**-G+	2.18	0.4
G+-**SS**-G−	2.15	0.4
G−-**SS**-G+	2.26	0.4
G−-**SS**-G−	2.18	0.4

[a] The first letter, A or G, refers to the orientation of the n-propyl group, the second letter, **A** or **S**, correspond to *anti* or *syn* orientation of the C═S with respect to the C—S, the third letter refers to the orientation of the S—C with respect to the C═O, and the last one describes the two possible orientation of the ethyl terminal group, anti (A) or gauche (G).
[b] Calculated from $\Delta G°$ according to the Boltzmann law, with 2 multiplicity for the *gauche* forms.

UV–visible spectroscopy

UV–visible spectra in the 200–800 nm range of solutions of the samples in solvents of different polarity and at different concentrations were recorded at room temperature on a Hewlett Packard UV–VIS spectrometer using a 1 cm-quartz cell.

Theoretical calculations

All of the quantum chemical calculations were performed with the Gaussian 03 program system [13], using the B3LYP method in combination with a 6-31+G* basis set. Geometry optimizations were sought using standard gradient techniques by simultaneous relaxation of all the geometrical parameters. The calculated vibrational properties correspond in all cases to potential energy minima for which no imaginary vibrational frequency was found. The electronic spectra were simulated using the TD-DFT formalisms over the previously optimized structures, with a maximum of 100 states and $S = 1$ [14,15].

Results and discussion

Mass spectra

The most intense peaks in the mass spectrum of CH_3-$OC(S)SC(O)OCH_2CH_3$ (Fig. S4) correspond to $m/z = 29$ ($CH_3CH_2^+$, 100%), $m/z = 75$ (CH_3OCS^+, ~90%), $m/z = 108$ ($CH_3OC(S)SH^+$, ~45%) and $m/z = 15$ (CH_3^+, ~30%). On the other hand, the most intense ionic fragment in the mass spectrum of both propyl derivatives (Figs. S5 and S6) is the propyl group, $C_3H_7^+$, at $m/z = 43$. This fact clearly denotes the higher stability of the R—O single bond for R = CH_3 compared with R = C_3H_7, when the molecules are exposed to electron impact ionization. A complete list of the peaks observed in the mass spectra of the three compounds, their relative abundances and their proposed assignment is presented as Supplementary material (Table S2). The parent ion, at $m/z = 180$ for R = CH_3 and at $m/z = 208$ for R = C_3H_7, is present in each of the spectra, allowing the identification of the samples.

$CH_3CH_2OC(O)SH$, obtained as a side-product of the reactions performed for the synthesis of the xanthogens, was clearly identified by its mass spectrum (presented in Fig. S7 and Table S3). The molecular ion was observed at $m/z = 106$, while the most intense peak corresponds to the $CH_3CH_2^+$ fragment ($m/z = 29$). Several signals could be also explained by rearrangement, being the

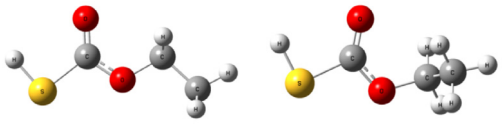

Fig. 1. Molecular models of the most stable conformers of $CH_3CH_2OC(O)SH$ calculated with the B3LYP/6-311++G** approximation (*syn* denotes the orientation of the C—S with respect to the C═O, and *anti* or *gauche* the conformation of the ethyl group).

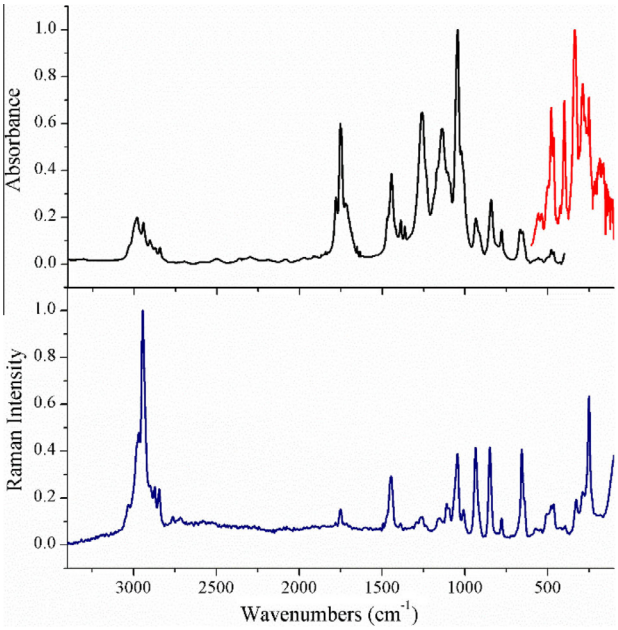

Fig. 2. IR (black trace between 3500 and 400 cm^{-1} and red trace between 600 and 100 cm^{-1}) and Raman (lower blue trace, between 3500 and 100 cm^{-1}) spectra of liquid $CH_3OC(S)SC(O)OCH_2CH_3$. (For interpretation of the references to color in this figure legend, the reader is referred to the web version of this article.)

$HOC(O)SH^+$ (m/z = 78) the most intense peak due to a McLafferty rearrangement.

NMR spectroscopy

The analysis of both ^1H and ^{13}C NMR spectra is important not only as purity criteria of the compounds but also as a structural characterization of the molecules. Table S4 lists ^1H NMR chemical shits, their multiplicities, and the ^3J values of the different signals for the three compounds. The comparison presented in this table serves to reinforce the proposed assignment and to verify the different listed ^3J values. Table S5 lists the corresponding ^{13}C NMR values for the three compounds. The ^1H and ^{13}C NMR spectra are shown in Figs. S8–S13. Again, the comparison of the values corroborates the assignment, the structure of the molecules and their purity.

Theoretical calculations

The structures and conformations of the molecules were theoretically investigated using DFT (B3LYP) and MP2 methods, mainly to help in the interpretation of the vibrational spectra in terms of different possible conformers in equilibrium. Considering the various dihedral angles of the compounds, several conformations are expected. Only the conformers laying 3 kcal/mol or less above the most stable structure were taking into account for the discussion, considering that higher-energy forms will not appreciable contribute to the population.

Starting from the —C(S)—S—C(O)— central moiety, two different conformations around each of the C—S single bond can be anticipated, as shown in Scheme 1. According with the calculations, the preferred structure is the one named **AS** in Scheme 1, this is the C=S double bond *anti* (**A**) with respect to the C—S single bond and the S—C single bond in *syn* (**S**) position with respect to the C=O double bond. This result is in agreement with the reported X-ray structure of $(CH_3)_2CHOC(S)SC(O)OCH_3$ [8]. The second and third conformers are structures named **AA** and **SS**, respectively, while the *syn-anti* form corresponds to a high energy conformer, and will not be considered. The dihedral angles around each C—O bond, τ_3 and τ_4 in Scheme 1, prefer the *syn* conformation. These C—O bonds have a double bond character, due to an electron delocalization, which explain the planarity of the R—O—C(S)—S—C(O)—O—Et moiety. Additionally to the three conformers previously described, the ethyl terminal group can adopt either *anti* or *gauche* conformation, giving a total number of six different structures. Figs. S14 and S15 of the Supplementary material depict the molecular models of the six conformers of $CH_3OC(S)SC(O)OCH_2CH_3$ and $(CH_3)_2CHOC(S)SC(O)OCH_2CH_3$, respectively, calculated with the B3LYP/6-31+G* approximation and Table 1 gives the theoretical relative energies and abundances.

The vibrational spectra (IR and Raman) were simulated for each of the conformers, to help in the interpretation of the experimental spectra. From the comparative analysis of the theoretical wavenumbers and relative IR and Raman intensities of the different conformers we can conclude that some of the vibrational modes are sensitive to the conformation adopted by the molecules, but not to the orientation of the ethyl group. For this reason, a relative abundance of each form –**SA**, **AA** and **SS**–, with independence of the conformation of the ethyl group, is also presented in Table 1.

The flexibility of the n-propyl group adds more conformational possibilities to the $CH_3(CH_2)_2OC(S)SC(O)OCH_2CH_3$ molecule with respect to the ones previously described. In addition to the *anti* or *gauche* conformation of the terminal ethyl group, the isopropyl moiety can also adopt either *anti* or *gauche* forms. For each of the three main conformers –**SA**, **AA** and **SS**– seven forms are expected, according with the orientation of both the terminal n-propyl and ethyl groups: A–A, A–G, G–A, G^+–G^+, G^+–G^-, G^-–G^+, and G^-–G^-. A total of 21 conformers, with relative stabilities below 3 kcal/mol with respect to the most stable form, were found according to the B3LYP/6-31+G* approximation. The relative energies and percentage of each form calculated at ambient temperature are presented in Table 2, and the molecular models are depicted in Fig. S16 of the Supplementary material. All of the structures correspond to true minima, with no imaginary frequencies in the calculated vibrational spectra.

Two conformers of $CH_3CH_2OC(O)SH$ are predicted to coexist at ambient temperature, differing in the orientation of the ethyl group, and with the SH single bond *syn* with respect to the C=O double bond. Fig. 1 shows the molecular models of the two conformers calculated with the B3LYP/6-311++G** approximation. The most stable form presents the ethyl group in *anti* position, while the second conformer – with *gauche* orientation – is predicted 0.48 and 0.25 kcal/mol higher in energy, according with the B3LYP/6-311++G** and MP2/6-311++G** approximations, respectively. In accordance with the Boltzmann law, and taking into consideration the 2 multiplicity of the *gauche* form, almost equal amount of each conformer is predicted at ambient temperature(*syn-anti*:*syn-gauche* 59:41 and 58:42 for B3LYP and MP2 calculations, respectively).

Vibrational analysis

Fig. 2 shows the IR and Raman spectra of a liquid sample of $CH_3OC(S)SC(O)OCH_2CH_3$ and Table 3 lists the wavenumbers observed in these spectra and also in the IR of an Ar-isolated matrix. The assignment of the bands has been performed with the aid of the predictions of theoretical calculations and also by the comparison with related molecules [14,16–20]. Although the calculations were performed for the isolated molecule, and therefore ignoring the intermolecular interactions present in the liquid phase, the agreement between the experimental and theoretical spectra is very good.

Table 3
Experimental (IR and Raman) and theoretical (B3LYP/6-311++G**) vibrational wavenumbers (cm^{-1}) of $CH_3OC(S)SC(O)OCH_2CH_3$.

Experimental			B3LYP/6-311++G**[b]	Assignment[c]
FTIR liquid	FTRaman liquid	Ar-matrix[a]		
3034	3031		3167	$\nu_{as}(CH_3)_{methyl\ (AS)}$
2983			3106	$\nu_{as}(CH_2)_{ethyl\ (AS)}$
	2968		3103	$\nu_{as}(CH_2)_{methyl\ (AS)}$
2945	2946		3097	$\nu_{as}(CH_2)_{ethyl\ (AS)}$
2904	2899		3080	$\nu_{s}(CH_2)_{ethyl\ (AS)}$
2872	2872		3059	$\nu_{s}(CH_3)_{ethyl\ (AS)}$
2845	2846		3040	$\nu_{s}(CH_3)_{methyl\ (AS)}$
2762	2763			$\nu(C{=}O)_{(AS)} + \nu(O{-}CH_2)_{(AS)}$
1782	1781		1816	$\nu(C{=}O)_{(SS)}$
1751	1750	1763.1 1761.7 1760.4 1758.0	1805	$\nu(C{=}O)_{(AS)}$
1719	1717	1743.4 1741.1	1776	$\nu(C{=}O)_{(AA)}$
1472	1474	1481.0	1488	$\delta(CH_2)_{ethyl\ (AS)}$
1444	1445	1451.3 1449.6 1448.8 1446.1 1445.0	1480	$\delta(CH_3)_{ethyl\ (AS)}$
1258	1258	1264.6 1263.3	1285	$\nu(C{-}O)_{[O-C(S)]\ (AS)}$
1138	1130	1143.8	1154	$\nu(C{-}O)_{[O-C(O)]\ (AS\text{-}A)}$
		1130.8 1128.2	1139	$\nu(C{-}O)_{[O-C(O)]\ (AS\text{-}G)}$
1044	1044	1065.5 1062.6 1054.9	1062	$\nu(C{=}S)_{(AS)}$
1010	1008		1026	$\nu(O{-}CH_2)_{(AS)}$
935	935	962.0 960.0 952.6	941	$\nu(O{-}CH_3)_{(AS)}$
779	779		846	$\rho(CH_3)_{(AS)}$
557	573		658	$\delta_{oop}(C{=}O)_{(AS)}$
537	540		566	$\delta_{oop}(C{=}S)_{(AS)}$
499	508		507	$\nu_{s}C{-}S{-}C_{(AS)}$
479	477		470	$\nu_{as}C{-}S{-}C_{(AS\text{-}G)}$
464	464		453	$\nu_{as}C{-}S{-}C_{(AS\text{-}A)}$
399	393		391	$\delta(O{-}C{-}C)_{ethyl\ (AS)}$
335	327		338	$\delta(S{-}C{-}O)_{(AS)}$
289	287		282	$\tau(C{-}C{-}O{-}C)_{(AS\text{-}G)}$
249	250		258	$\tau(C{-}C{-}O{-}C)_{(AS\text{-}A)}$

[a] Different matrix sites are indicated between the key symbol.
[b] The wavenumber of the most stable form of each group is listed.
[c] AS, AA, SS, AS-A and AS-G denote the conformers defined in Table 1 and Fig. S14.

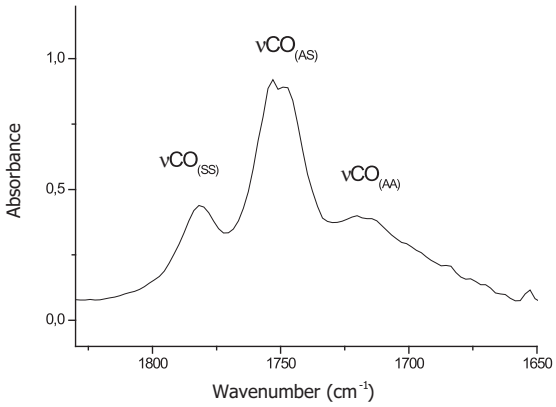

Fig. 3. IR spectra of liquid $CH_3OC(S)SC(O)OCH_2CH_3$ between 1830 and 1650 cm^{-1}.

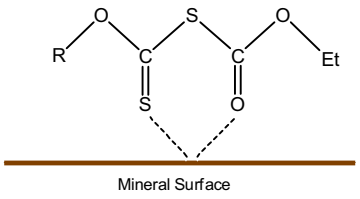

Scheme 2. Schematic representation of the potential chelating ability of the **SS** conformer of ROC(S)SC(O)OEt molecules during a flotation process.

As previously reported for similar molecules [14,15,18], the carbonylic stretching mode can be considered as a conformational sensor. In this case, three bands are clearly observed in the IR spectrum of liquid $CH_3OC(S)SC(O)OCH_2CH_3$ (see Fig. 3), at 1782, 1751 and 1719 cm^{-1}. The same pattern is present in the Raman spectrum. According to the theoretical vibrational shifts, and also considering the predicted relative abundances of the different conformers, these bands were assigned to the **SS**, **SA**, and **AA** conformers, respectively (see Table 3). On the other hand, the conformation adopted by the terminal ethyl group has no influence in the carbonylic wavenumber. The IR spectrum of the molecule isolated in solid Ar, that freeze at approximately 15 K the conformational composition of the gas phase at ambient temperatures, shows only two absorptions, with their corresponding matrix-site

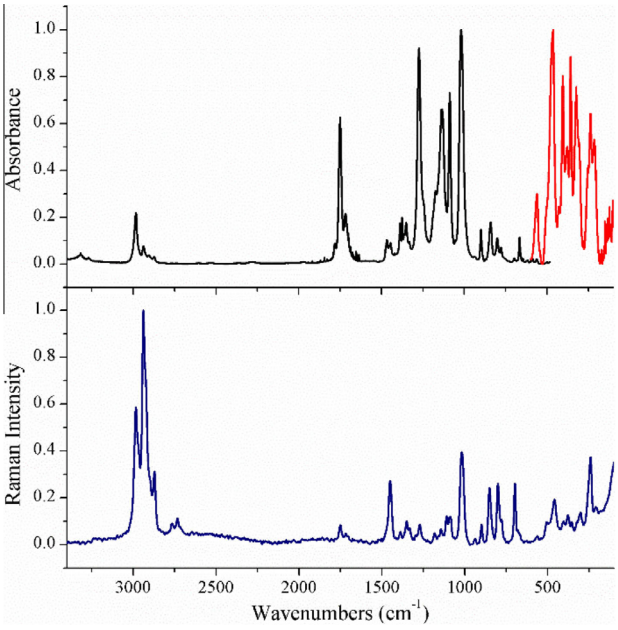

Fig. 4. IR (black trace between 3500 and 400 cm^{-1} and red trace between 600 and 100 cm^{-1}) and Raman (lower blue trace, between 3500 and 100 cm^{-1}) spectra of liquid $(CH_3)_2CHOC(S)SC(O)OCH_2CH_3$. (For interpretation of the references to color in this figure legend, the reader is referred to the web version of this article.)

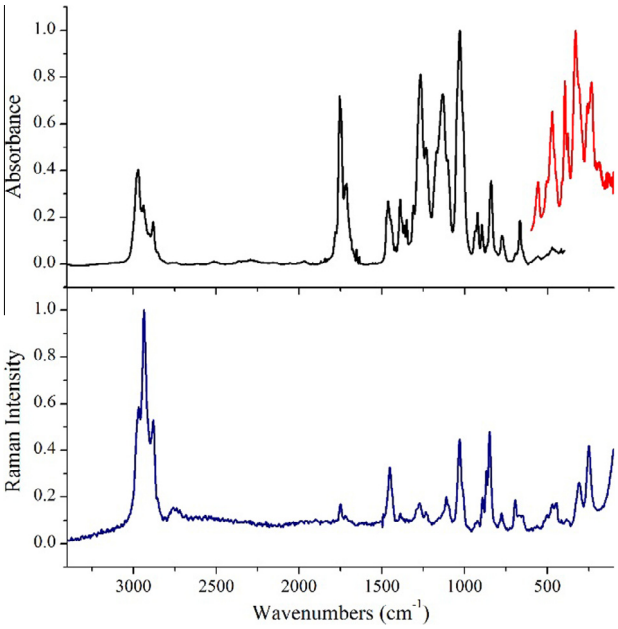

Fig. 5. IR (black trace between 3400 and 400 cm^{-1} and red trace between 600 and 100 cm^{-1}) and Raman (lower blue trace, between 3400 and 100 cm^{-1}) spectra of liquid $CH_3(CH_2)_2OC(S)SC(O)OCH_2CH_3$. (For interpretation of the references to color in this figure legend, the reader is referred to the web version of this article.)

splitting. These bands, at 1763 and 1743 cm^{-1}, were assigned to the **SA** and **AA** conformers, while no signs of the third **SS** form were observed. The relative high intensity of the carbonylic absorption of the **SS** conformer in the liquid IR spectra compared with its predicted relative abundance, together with their absence in the IR matrix isolated spectrum, suggests the stabilization of this form in the liquid phase by, presumably, intermolecular interactions. According with the discussion presented in the introduction of this paper, the **SS** form would be the most appropriated conformer to act as a chelating agent in the flotation process, as schematically shown in Scheme 2.

Table 4
Experimental (IR and Raman) and theoretical (B3LYP/6-31+G*) vibrational wavenumbers (cm^{-1}) of $(CH_3)_2CHOC(S)SC(O)OCH_2CH_3$.

Experimental		B3LYP/6-31 + G*	Assignment[a]
FTIR liquid	FTRaman liquid		
3319			$2\nu(C{=}O)_{(AS)}$
3267			$2\nu(C{=}O)_{(AA)}$
2983	2984	3141	$\nu_{as}(CH_2)_{ethyl\ (AS)}$
	2969	3139	$\nu_{as}(CH_3)_{isopropyl\ (AS)}$
2938	2939	3129	$\nu_{as}(CH_2)_{ethyl\ (AS)}$
	2926	3125	$\nu_{as}(CH_3)_{isopropyl\ (AS)}$
2905	2900	3080	$\nu_s(CH_2)_{ethyl\ (AS)}$
2873	2873	3059	$\nu_s\ (CH_3)_{ethyl\ (AS)}$
	2767	3058	$\nu_s(CH_3)_{isopropyl\ (AS)}$
	2733	3056	$\nu_s(CH_3)_{isopropyl\ (AS)}$
1781	1783	1814	$\nu(C{=}O)_{(SS)}$
1748	1750	1803	$\nu(C{=}O)_{(AS)}$
1716	1718	1775	$\nu(C{=}O)_{(AA)}$
{ 1466	1451	1519	$\delta(CH_3)_{ethyl\ (AS)}$
{ 1445			
1386	1387	1516	$\delta(CH_2)_{ethyl\ (AS)}$
1374		1509	$\delta(CH_3)_{isopropyl\ (AS)}$
1351	1350	1395	$\delta(H{-}C{-}O)_{(AS)}$
1333	1332	1376	$\delta(H{-}C{-}CH_3)_{(AS)}$
1273	1271	1310	$\nu(C{-}O)_{[O-C(S)]\ (AS)}$
1244		1306	$\nu(C{-}O)_{[O-C(S)]\ (AA)}$
1172	1182	1173	$\nu(C{-}O)_{[O-C(O)]\ (AS\text{-}A)}$
1134	1144	1158	$\nu(C{-}O)_{[O-C(O)]\ (AS\text{-}G)}$
1087	1086	1124	$\nu(C{-}O)_{[O-isopropyl]\ (AS)}$
1018	1017	1025	$\nu(C{=}S)_{(AS)}$
899	899	1019	$\nu(O{-}CH_2)_{(AS)}$
874		912	$\nu_s(C{-}C{-}C)_{(AS)}$
840	850	872	$\nu(C{-}S)_{[C(O)-S]\ (AS)}$
800	799	843	$\rho(CH_3)_{(AS)}$
777	778	806	$\rho(CH_3)_{(AS)}$
697	697	783	$\nu(C{-}S)_{[C(S)-S]\ (AS)}$
666	667	667	$\delta_{oop}(C{=}O)_{(AS)}$
562	562	567	$\delta_{oop}(C{=}S)_{(AS)}$
500	505	501	$\delta(O{-}C{-}S)_{(AS)}$
464	458	475	$\delta(O{-}C{-}C)_{ethyl\ (AS)}$
404	403	461	$\delta(O{-}C{-}C)_{isopropyl\ (AS)}$
378	378	457	$\delta(C{-}C{-}C)_{isopropyl\ (AS)}$
358	354	400	$\delta(O{-}C{-}C)_{ethyl\ (AS)}$
324	322	378	$\delta(O{-}C{-}S)_{(AS)}$
306	300	324	$\delta(S{-}C{-}O)_{(AS)}$
238	241	294	$\tau(C{-}C{-}O{-}C)_{(AS)}$
212	210	234	$\tau(C{-}O{-}C{=}S)_{(AS)}$

[a] AS, AA, SS, AS-A and AS-G denote the conformers defined in Table 1 and Fig. S15.

Some vibrational modes are also sensitive to the conformation adopted for the terminal ethyl group. For example, two bands are observed for $\nu(C{-}O)_{[O-C(O)]}$, $\nu_{as}C{-}S{-}C$, and $\tau(C{-}C{-}O{-}C)$, attributable to the **SA-A** and **SA-G** conformers, as listed in Table 3.

The position of the vibration modes assigned to the stretching of the four C—O single bonds of the molecule follows the following trend:

$$\nu(C-O)_{[O-C(S)]} > \nu(C-O)_{[O-C(O)]} > \nu(C-O)_{[O-CH_2]} > \nu(C-O)_{[O-CH_3]}.$$

This trend denotes the double bond character of the CO bonds attached to the thiocarbonylic group, in major extent, and also to the carbonylic group, due to electronic delocalization.

Figs. 4 and 5 present the IR and Raman spectra of a liquid sample of $ROC(S)SC(O)OCH_2CH_3$, with R = isopropyl— and *n*-propyl—, respectively, while the experimental wavenumbers, together with the predicted ones and a tentative assignment, are listed in Tables 4 and 5. As presented above for the methyl derivative, and based on the purity of the compounds determined either by GC–MS and NMR analysis, the vibrational spectra can be interpreted only if a mixture of different conformers in equilibrium is considered

Table 5
Experimental (IR and Raman) and theoretical (B3LYP/6-31 + G*) vibrational wavenumbers (cm^{-1}) of $CH_3(CH_2)_2OC(S)SC(O)OCH_2CH_3$.

Experimental		B3LYP/6-31 + G*	Assignment[a]
FTIR liquid	FTRaman liquid		
2979	2982	3144	$\nu_{as}(CH_2)_{ethyl\ (AS)}$
2971		3127	$\nu_{as}(CH_2)_{npropyl\ (AS)}$
	2969	3125	$\nu_{as}(CH_3)_{npropyl\ (AS)}$
2939	2937	3120	$\nu_{as}(CH_2)_{ethyl\ (AS)}$
2926		3106	$\nu_{as}(CH_2)_{npropyl\ (AS)}$
2906		3081	$\nu_{s}(CH_2)_{ethyl\ (AS)}$
2881	2880	3058	$\nu_{s}(CH_3)_{ethyl\ (AS)}$
2854	2855	3043	$\nu_{s}(CH_3)_{nPropyl\ (AS)}$
1782		1816	$\nu\ (C{=}O)_{(SS)}$
{ 1755 / 1745	1749	1804	$\nu\ (C{=}O)_{(AS)}$
{ 1723 / 1711	{ 1719 / 1713	1777	$\nu\ (C{=}O)_{(AA)}$
1473	1470	1535	$\delta(CH_2)_{ethyl\ (AS)}$
1464		1524	$\delta(CH_2)_{npropyl\ (G\text{-}AS)}$
1456	1451	1520	$\delta(CH_2)_{npropyl\ (A\text{-}AS)}$
1444		1514	$\delta(CH_3)_{ethyl\ (AS)}$
1437	1436	1508	$\delta(CH_3)_{npropyl\ (A\text{-}AS)}$
1419		1500	$\delta(CH_3)_{npropyl\ (G\text{-}AS)}$
1389	1389	1444	$\delta(CH_2)_{ethyl\ (AS)}$
1377	1379	1438	$\delta(CH_3)_{npropyl\ (AS)}$
1364	1365	1407	$\delta(CH_2)_{ethyl\ (AS)}$
1350	1352	1395	$\delta(CH_2)_{npropyl\ (AS)}$
1309	1308.2	1327	$\delta(CH_2)_{npropyl\ (AS)}$
	1294	1304	$\delta(CH_2)_{ethyl\ (AS)}$
1279	1273	1300	$\nu(C{-}O)_{[O\text{-}C(S)]\ (AS)}$
1267	1268	1296	$\nu(C{-}O)_{[O\text{-}C(S)]\ (AA)}$
	1234	1276	$\delta(CH_2)_{npropyl\ (AS)}$
1233	1223.8	1265	$\nu(C{-}O)_{[O\text{-}C(S)]\ (SS)}$
1171		1200	$\nu(C{-}O)_{[O\text{-}C(O)]\ (AA)}$
1133	1132	1174	$\nu(C{-}O)_{[O\text{-}C(O)]\ (AS)}$
1105	1110	1150	$\nu_{s}(C{-}C{-}C)_{(AS)}$
	1094	1140	$\rho(CH_2)_{ethyl\ (AS)}$
1048		1052	$\nu_{as}(C{-}C{-}C)_{(AS)}$
1029	1030	1039	$\nu(C{=}S)_{(AS)}$
1011	1010	1036	$\nu(C{-}C)_{ethyl\ (AS)}$
937	935	955	$\nu(O{-}C)_{npropyl\ (A\text{-}AS)}$
923	922	940	$\nu(O{-}C)_{npropyl\ (G\text{-}AS)}$
896	892	909	$\rho(CH_2)_{npropyl\ (AS)}$
867	868	872.7	$\nu(O{-}C)_{ethyl\ (AS)}$
841	849	843	$\nu(C{-}S)_{[C(O)\text{-}S]\ (AS)}$
	793	818	$\rho(CH_2)_{ethyl\ (AS)}$
776	777	781	$\rho(CH_2)_{npropyl\ (G\text{-}AS)}$
	761	769	$\rho(CH_2)_{npropyl\ (A\text{-}AS)}$
694	694	706	$\nu(C{-}S)_{[C(S)\text{-}S]\ (A\text{-}AS)}$
	672	682	$\nu(C{-}S)_{[C(S)\text{-}S]\ (G\text{-}AS)}$
{ 669 / 665	662	666	$\delta_{oop}(C{=}O)_{(AS)}$
558		567	$\delta_{oop}(C{=}S)_{(AS)}$
507	521	504	$\delta(O{-}C{-}S)_{(AS)}$
471	469	463	$\delta(O{-}C{=}S)_{(AS)}$
458		455	$\delta(C{-}C{-}C)_{(AS)}$
419	415	411	$\delta(C{-}C{-}O)_{ethyl\ (AS\text{-}A)}$
396		386	$\delta(C{-}C{-}O)_{ethyl\ (AS\text{-}G)}$
379		372	$\delta(O{-}C{-}C)_{npropyl\ (AS)}$
331.5		325	$\delta(O{-}C{-}S)_{(AS)}$
307	308.7	309	$\delta(S{-}C{-}O)_{(AS)}$
	249	250	$\tau\ (C{-}C{-}O{-}C)_{(AS)}$

[a] AS, AA, SS, A-AS, G-AS, AS-A and AS-G denote the conformers defined in Table 2 and Fig. S16.

Table 6
Comparison of the IR wavenumbers of the most stable conformers of $ROC(S)SC(O)OCH_2CH_3$, with R = CH_3—, $(CH_3)_2CH$—, and $CH_3(CH_2)_2$—.

R	ν(C=O)	ν(C=S)	$\nu(C{-}O)_{[O\text{-}C(S)]}$	$\nu(C{-}O)_{[O\text{-}C(O)]}$
CH_3—	1751	1044	1258	1138
$(CH_3)_2CH$—	1748	1018	1273	1134
$CH_3(CH_2)_2$—	1745	1029	1279	1133

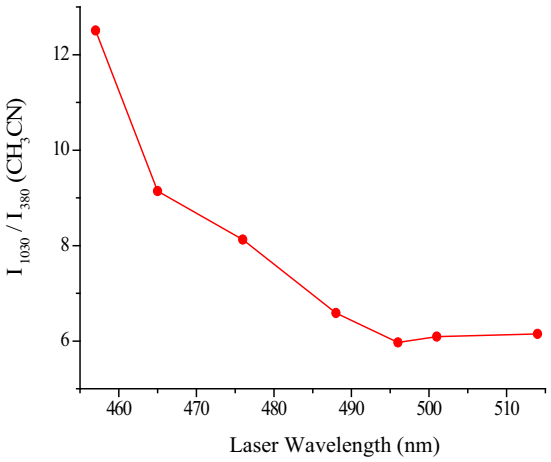

Fig. 6. Raman excitation profile of the 1030 cm^{-1} band assigned to ν(C=S) of $CH_3(CH_2)_2OC(S)SC(O)OCH_2CH_3$ with respect to the 380 cm^{-1} band of CH_3CN.

(see Figs. S15 and S16). Again, the carbonylic stretching spectral regions present the more clear evidence of the presence of the three groups of conformers in liquid phase: **AS**, **AA**, and **SS**. The matrix IR spectrum of $(CH_3)_2CHOC(S)SC(O)OCH_2CH_3$ shows only signals of the **AS** conformers (see Table 4). From the theoretical results presented in Table 1, the relative stabilities of the second group of conformers (**AA**) are smaller for the isopropyl derivative than for the methyl one. On the other hand, the stabilization of conformers **AA** and **SS** in liquid phase compared with gas phase becomes evident.

The vibrational (IR and Raman) spectra of $CH_3(CH_2)_2$-$OC(S)SC(O)OCH_2CH_3$ are composed mainly by signals arising from the **AS** conformer, with some of the bands, as for example in the ν(C=O) spectral region, originated by the **AA** and **SS** forms. In some cases, bands corresponding to the A-**AS**, G-**AS**, **AS**-A and **AS**-G conformers can be distinguished. A complete list of the wavenumbers and a tentative assignment is presented in Table 5.

Table 6 shows a comparison of the IR vibrational bands assigned to the C=O, C=S, O—C(S), and O—C(O) stretching modes in the liquid IR spectra of the three compounds. As can be observed in the table, the values are very similar. The main difference is noticed for the ν(C=S) mode of the methyl derivative, observed at higher wavenumbers, denoting a stronger bond than in the other two compounds. The $\nu(C{-}O)_{[O\text{-}C(S)]}$ follows the opposite trend.

Pre-resonance Raman spectroscopy

The resonance or pre-resonance Raman effect was investigated for $CH_3(CH_2)_2OC(S)SC(O)OCH_2CH_3$. Raman spectra of 1:1 mixtures of the compound with CH_3CN, used as internal standard, were taken using eight different excitation lines of an Ar laser between 528.7 and 457.9 nm. The intensity of the band assigned to ν(C=S), at 1030 cm^{-1}, presents a moderated enhancement as the excitation energy increases. Fig. 6 depicts the pre-resonance excitation profile of the 1030 cm^{-1} band with respect to the 380 cm^{-1} band of CH_3CN. This pre-resonant behavior is associated with an electronic absorption observed at 376 nm, and assigned to the $n \rightarrow \pi^*$ of the C=S chromophore.

Electronic spectroscopy

The UV–visible spectra of the three compounds were measured in solutions of several concentrations in solvents with different polarities (carbon tetrachloride, ethylic ether, chloroform, acetone, methanol, and acetonitrile). A complete list of the absorption

Table 7
Comparison of the experimental absorption maxima (λ, nm) and extinction coefficients (ε, L mol^{-1} cm^{-1}) of the UV–visible spectra of ROC(S)SC(O)OCH$_2$CH$_3$, with R = CH$_3$—, (CH$_3$)$_2$CH—, CH$_3$(CH$_2$)$_2$— with the energy and oscillator strength of the electronic transitions calculated with the TD-B3LYP/6-31+G(d) approximation.

Transition	$n \rightarrow \pi^*$ (C=S)	$\pi \rightarrow \pi^*$ (C=S)	$\pi \rightarrow \pi^*$ (C=S)	$\pi \rightarrow \pi^*$ (C=O)
CH$_3$OC(S)SC(O)OCH$_2$CH$_3$				
λ_{exp} [mn][a]	361	298	273	216
(ε_{exp} [L mol^{-1} cm^{-1}])[a]	(100)	(20·10^3)	–[b]	(10·10^3)
λ_{theor} [mn]	362	260	188	150
(Oscillator strength)	(11·10^{-4})	(20·10^{-2})	(89·10^{-3})	(13·10^{-2})
(CH$_3$)$_2$CHOC(S)SC(O)OCH$_2$CH$_3$				
λ_{exp} [mn][a]	376	302	276	224
(ε_{exp} [L mol^{-1} cm^{-1}])[a]	(54)	(15·10^3)	(16·10^3)	(12·10^3)
λ_{theor} [mn]	366	262	193	179
(Oscillator strength)	(14·10^{-4})	(19·10^{-2})	(10·10^{-2})	(10·10^{-2})
CH$_3$(CH$_2$)$_2$C(S)SC(O)OCH$_2$CH$_3$				
λ_{exp} [mn][c]	376	272		220
(ε_{exp} [L mol^{-1} cm^{-1}])[c]	(43)	(88·10^2)		(53·10^2)
λ_{theor} [mn]	354	259		209
(Oscillator strength)	(1·10^{-4})	(19·10^{-2})		(9·10^{-2})

[a] Taken from the spectrum measured in methanol solutions.
[b] The experimental ε could not be measured due to overlap of the bands.
[c] Taken from the spectrum measured in acetonitrile solutions.

Table 8
Energy (eV) and approximate character of selected molecular orbitals calculated using the NBO analysis at the B3LYP/6-31+G* level of approximation for the most stable **SS** conformers of ROC(S)SC(O)OCH$_2$CH$_3$, with R = CH$_3$—, CH$_3$CH$_2$—, (CH$_3$)$_2$CH—, and CH$_3$(CH$_2$)$_2$—.

MO	Character	CH$_3$—	CH$_3$CH$_2$—	(CH$_3$)$_2$CH—	CH$_3$(CH$_2$)$_2$—
LUMO+1	π^*(C=O)	−0.58639	−0.62149	−0.65197	−0.61414
LUMO	π^*(C=S)	−2.30992	−2.33580	−2.38828	−2.31917
HOMO	n_pS	−5.85738	−5.91806	−5.96703	−5.90527
HOMO-2	n_pO	−7.68267	−7.71695	−7.75641	−7.69981

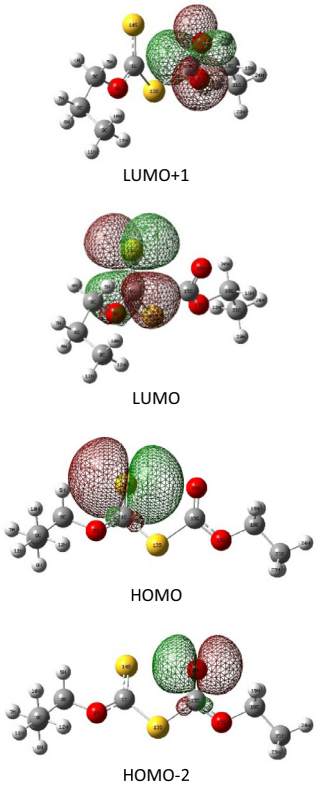

Fig. 7. Schematic representation of selected molecular orbitals of CH$_3$(CH$_2$)$_2$-OC(S)SC(O)OCH$_2$CH$_3$ calculated using the NBO analysis at the B3LYP/6-31+G* level of approximation.

maxima and the calculated absorption coefficients are listed in Table S6, and some of the spectra are presented in Fig. S17.

To help in the interpretation and assignment of the absorption maxima to the electronic transitions of the molecules, TD-DFT calculations were performed. The calculated electronic spectra are almost invariable for the different conformers of each compound. For this reason, only the data corresponding to the most stable form of each molecule are presented. Table 7 compares the experimental maxima with the calculated ones using the TD-B3LYP/6-31+G(d) approximation. The strongest absorptions corresponds to $\pi \rightarrow \pi^*$ transitions localized at the C=O and C=S groups. A weak absorption, appearing at 361 nm for the compound with R = CH$_3$— and at 376 nm for each of the propyl derivatives, is assigned to an $n \rightarrow \pi^*$ electronic transition localized at the C=S group, according with the TD-DFT calculations, and also in agreement with the assignment for related molecules [16]. The Raman enhancement of the C=S stretching vibrational mode in pre-resonance with this electronic transition reinforces the assignment.

Considering that the energy and character of the HOMO and LUMO orbitals of xanthogen compounds are proposed to be very important for the evaluation of the reactivity, selectivity, and collector ability of the molecules [5], these orbitals were predicted using the NBO analysis. Only the **SS** conformers were evaluated, since the flotation process occur most probably through these forms, the only ones that present the possibility to form a six member ring (see Scheme 2). Table 8 lists the energy of four frontier orbitals calculated with the B3LYP/6-31+G* approximation, selected as the most important ones to evaluate the interaction of the molecules with the mineral surface, of the three compounds studied in this work. Fig. 7 depicts the schematic representation of these molecular orbitals calculated for CH$_3$(CH$_2$)$_2$OC(S)SC(O)OCH$_2$-CH$_3$. For comparison purposes, the ethyl derivative was also included in the table. The interaction between the xantogens and the mineral surface occurs mainly through lone electron pairs located at the sulfur and oxygen atoms of the C=S and C=O groups. The HOMO and HOMO-2 orbitals, assigned to n_pS and n_pO, respectively, are then the most relevant ones to evaluate their reactivity. The higher the energy of the HOMO and/or HOMO-2 orbitals, the greater the ability and selectivity of the xanthogen molecule to form a covalent bond. On the other hand, the LUMO and LUMO+1 orbitals, with π^*(C=S) and π^*(C=O) character, are also important for the interaction with d-orbitals of the metal. According with the data listed in Table 8, the collector selectivity will be

Table 9
Band position (in cm^{-1}) and assignment of the IR absorptions appearing after photolysis of $CH_3OC(S)SC(O)OCH_3$ isolated in solid Ar.

Ar-matrix	Molecule	Vibrational mode	Wavenumber reported previously
2346.3 2340.2	CO_2	$\nu_{as}(O{=}C{=}O)$	2344.7 [a] 2339.1
2141.0 2138.2 2136.6	CO	$\nu(CO)$	2138.2 [b]
2057.5 2056.1 2054.9 2052.7 2049.7 2046.9 2044.3	OCS	$\nu(C{=}O)$	2049.3 [c]
1800.5 1797.8 1795.6 1793.0	$CH_3CH_2OC(O)SH$	$\nu(C{=}O)$	This work
1718.0	CH_2O	$\nu(C{=}O)$	1742.0 [d]
1533.8 1532.3 1531.0 1527.6 1524.2 1521.1	CS_2	$\nu_{as}(S{=}C{=}S)$	1528.6 [e]
1387.5	$CH_3CH_2OC(O)SH$	$\delta(CH_3)$	This work
1355.2 1354.0	SO_2	$\nu_{as}(SO_2)$	1355.6 [f] 1355.1
1351.2	$CH_3CH_2OC(O)SH$	$\delta(CH_3)$	This work
1334.0	SO_2	$\nu_{as}(^{34}SO_2)$	1339.6 [f] 1335.1
1239.6	CH_2O	$\delta(H{-}C{-}O)$	1245.1 [d]
1216.5	$CH_3CH_2OC(O)SH$	$\delta(CH_2)$	This work
1183.0 1179.0 1169.4	CH_2O	$\nu(C{-}O)$	1168.0 [d]
1123.4 1122.3 1121.3 1120.5 1119.5 1118.5	$CH_3CH_2OC(O)SH$	$\delta(CH_2)$	This work
1110.0 1107.7 1106.2 1103.5	$CH_3CH_2OC(O)SH$	$\nu(C{-}O)_{[O-C(O)]}$	This work
1025.7 1024.0	$CH_3CH_2OC(O)SH$	$\nu(C{-}O)_{[O-CH2]}$	This work
843.6 841.9	$CH_3CH_2OC(O)SH$	$\delta(S{-}H)$	This work
843.6 841.9	$CH_3CH_2OC(O)SH$	$\delta_{oop}(S{-}H)$	This work
667.7 666.9	$CH_3CH_2OC(O)SH$	$\delta_{oop}(C{=}O)$	This work
663.6 661.9	CO_2	$\delta(O{=}C{=}O)$	663.8 663.5 [a] 662.0

[a] Ref. [23].
[b] Ref. [24].
[c] Refs. [26,27].
[d] Ref. [21].
[e] Ref. [25].
[f] Ref. [28].

$CH_3- > CH_3(CH_2)_2- > CH_3CH_2- > (CH_3)_2CH-$. The selectivity of some of this compounds were experimentally determined, concluding that $CH_3CH_2- > (CH_3)_2CH-$ for $ROC(S)SC(O)OCH_2CH_3$, which is in accordance with our predictions.

Matrix photochemistry

An Ar-matrix of $CH_3OC(S)SC(O)OCH_2CH_3$ was irradiated with broad-band light ($200 \leqslant \lambda \leqslant 800$ nm) and the photolysis products were identified by their IR spectra, taken at different irradiation times. Absorptions at 1800.5/1797.8/1795.5/1793.0 and 1110.0/1107.7/1106.2/1103.5 cm^{-1} were clearly formed and grown on photolysis. From the analysis of all of the new IR signals observed in the IR matrix spectra against the irradiation time, seven other absorptions were found to follow the same kinetic pattern (see Table 9). The formation of $CH_3CH_2OC(O)SH$ was proposed to explain the experimental findings in the IR spectra. As mention in the introduction, as far as we know, no previous report of this molecule was found in the literature. The IR wavenumbers were compared with the ones observed in the liquid IR spectrum of a sample obtained in this work as a side-product of the xanthogen synthesis, and also with theoretical predictions. The experimental and theoretical wavenumbers, together with the proposed assignment were listed in Table 10. Formaldehyde was also identified as a photoproduct, by comparison of the 1718.0, 1239.6 and 1183.0/1179.0/1169.4 cm^{-1} absorptions with Ar-matrix literature values (see Table 9) [21].

Based on the identified photoproducts, the proposed photochemical mechanism of $CH_3OC(S)SC(O)OCH_2CH_3$ isolated in Ar-matrix was depicted in Scheme 3. Similar mechanisms were previously reported for other molecules possessing a methyl group and also a divalent sulfur atom, as for example $CH_3C(O)SX$, with X = H—, CH_3— or $CH_3C(O)$— [18]. No evidence of the CS molecule, which IR absorption is expected in the 1280 cm^{-1} spectral region, is observed in the spectra taken after photolysis. However, the lack of this band can be attributed to the low intensity of the vibrational mode of this molecule in the IR spectrum [22].

Additionally, CO_2 [23], CO [24], CS_2 [25], OCS [26,27] and SO_2 [28] were identified through their characteristic Ar-matrix IR bands, presumably arising from secondary photochemical channels.

Table 10
Experimental (liquid and Ar-matrix IR) and theoretical (B3LYP/6-311++G**) vibrational wavenumbers (cm^{-1}) of $CH_3CH_2OC(O)SH$.

Experimental		B3LYP/6-311++G**	Assignment
FTIR liquid	FTIR Ar-matrix [a]		
2984		3120.5	$\nu_{as}(CH_3)$
1790	1800.5 1797.8 1795.6 1793.0	1779.8	$\nu(C{=}O)$
1386	1387.5	1485.7	$\delta(CH_3)$
	1351.2	1426.6	$\delta(CH_3)$
	1216.5	1327.3	$\delta(CH_2)$
	1123.4 1122.3 1121.3 1120.5 1119.5 1118.4	1196.9	$\delta(CH_2)$
1103	1110.0 1107.7 1106.2 1103.5	1180.3	$\nu(C{-}O)_{[O-C=O]}$
1022	1025.7 1024.0	1035.1	$\nu\ (C{-}O)_{[O-CH2]}$
840	843.6 841.9	951.6	$\delta_{oop}(S{-}H)$
666	667.7 666.9	677.7	$\delta_{oop}(C{=}O)$

[a] Different matrix sites are indicated between the key symbol.

Conclusions

The conformational properties of three xanthogen ethyl formates of general formula $ROC(S)SC(O)OCH_2CH_3$, with R = CH_3—, $(CH_3)_2CH$— and $CH_3(CH_2)_2$—, were studied using theoretical

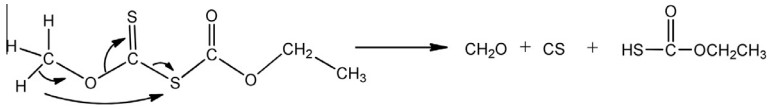

Scheme 3. Proposed photolysis main mechanism for $CH_3OC(S)SC(O)OCH_2CH_3$ isolated in solid Ar.

methods and spectroscopic techniques. For all of the compounds the preferred conformation of the ROC(S)SC(O)OEt moiety was **AS** – the C═S double bond *anti* with respect to the C—S single bond and the S—C single bond *syn* with respect to the C═O double bond – followed by **AA** and **SS** conformers. Furthermore, the two conformational possibilities of the ethyl and n-propyl substituents add more forms to the conformational space, giving a total of 6 conformers for R = CH_3— and $(CH_3)_2CH$—, and 21 for R = $CH_3(CH_2)_2$—.

The vibrational spectra (IR, Raman, and matrix-IR) of the molecules are consistent with the presence of the three groups of conformers, **AS**, **AA**, and **SS**, and can be considered as an experimental proof of the conformational equilibrium. Only some vibrational modes are sufficiently split to discern the contribution of the individual conformers in the vibrational spectra, being the ν(C═O) vibrational modes the most dependent on the conformation. Some modes are also affected by the rotameric form adopted either by the ethyl or the n-propyl terminal groups.

From the comparison of the liquid and matrix-isolated IR spectra, the stabilization of the **SS** form in the liquid phase, presumably by intermolecular interactions, becomes evident. The chelating capabilities of these molecules, important in the mineral flotation processes, will be enhanced for the **SS** conformer, since the two interaction centers, the S and O atoms of the C═S and C═O groups, can coordinate the metal site simultaneously, forming a very stable six-member ring.

The UV–visible photochemistry of the smallest congener of the series, $CH_3OC(S)SC(O)OCH_2CH_3$, was studied in matrix isolation conditions. The previously unknown molecule, $CH_3CH_2OC(O)SH$, was produced in the main photochemical channel, and characterized by its matrix-isolated IR spectra. This compound was also obtained in this work as a side-product of the reaction between potassium xanthate salts, ROC(S)SK, and ethyl chloroformate, $ClC(O)OCH_2CH_3$. It was characterized by its mass and IR spectrum. Although $CH_3CH_2OC(O)SH$ was not previously reported, their salts were proposed as a decomposition product during the flotation processes.

Acknowledgements

The authors thank the Consejo Nacional de Investigaciones Científicas y Técnicas (CONICET) (PIP 4695), the Agencia Nacional de Promoción Científica y Tecnológica (PICT 0647) and the Facultad de Ciencias Exactas, Universidad Nacional de La Plata (UNLP – 11/X684), for financial support.

Appendix A. Supplementary data

Supplementary data associated with this article can be found, in the online version, at http://dx.doi.org/10.1016/j.saa.2014.12.086.

References

[1] W.A. Douglass, United States Patent, 1.652.099 A, 1927.
[2] A.H. Fischer, United States Patent, 1.684.536, 1928.
[3] P.K. Ackerman, G.H. Harris, R.R. Klimpel, F.F. Aplan, Int. J. Miner. Process. 58 (2000) 1.
[4] P.K. Ackerman, G.H. Harris, R.R. Klimpel, F.F. Aplan, Int. J. Miner. Process. 21 (1987) 105.
[5] F. Yang, W. Sun, Y. Hu, Miner. Eng. 39 (2012) 140.
[6] H. Yekeler, M. Yekeler, Appl. Surf. Sci. 236 (2004) 435.
[7] S. Wei, Y. Fan, H. Yue-Hua, H. Guo-Yong, L. Wen-Li, Chin. J. Nonferrous Met. 19 (2009) 8.
[8] Y.A. Tobón, R.M. Romano, E. Hey-Hawkins, R. Boese, C.O. Della Védova, J. Phys. Org. Chem. 22 (2009) 815.
[9] E. Sylvester, D. Truccolo, F.P. Hao, J. Chem. Soc. Perkin Trans. 2 (9) (2002) 1562.
[10] M.H. Jones, J.T. Woodcock, Anal. Chim. Acta 193 (1987) 41.
[11] I.R. Dunkin, Matrix-Isolation Techniques: A Practical Approach, Oxford University Press, New York, 1998;
M.J. Almond, A.J. Downs, Adv. Spectrosc. 17 (1989) 1.
[12] R.N. Perutz, J. Turner, J. Chem. Soc. Faraday Trans. 2 (69) (1973) 452.
[13] M.J. Frisch, G.W. Trucks, H.B. Schlegel, G.E. Scuseria, M.A. Robb, J.R. Cheeseman, J.A. Montgomery Jr., T. Vreven, K.N. Kudin, J.C. Burant, J.M. Millam, S.S. Iyengar, J. Tomasi, V. Barone, B. Mennucci, M. Cossi, G. Scalmani, N. Rega, G.A. Petersson, H. Nakatsuji, M. Hada, M. Ehara, K. Toyota, R. Fukuda, J. Hasegawa, M. Ishida, T. Nakajima, Y. Honda, O. Kitao, H. Nakai, M. Klene, X. Li, J.E. Knox, H.P. Hratchian, J.B. Cross, C. Adamo, J. Jaramillo, R. Gomperts, R.E. Stratmann, O. Yazyev, A.J. Austin, R. Cammi, C. Pomelli, J.W. Ochterski, P.Y. Ayala, K. Morokuma, G.A. Voth, P. Salvador, J.J. Dannenberg, V.G. Zakrzewski, S. Dapprich, A.D. Daniels, M.C. Strain, O. Farkas, D.K. Malick, A.D. Rabuck, K. Raghavachari, J.B. Foresman, J.V. Ortiz, Q. Cui, A.G. Baboul, S. Clifford, J. Cioslowski, B.B. Stefanov, G. Liu, A. Liashenko, P. Piskorz, I. Komaromi, R.L. Martin, D.J. Fox, T. Keith, M.A. Al-Laham, C.Y. Peng, A. Nanayakkara, M. Challacombe, P.M.W. Gill, B. Johnson, W. Chen, M.W. Wong, C. Gonzalez, J.A. Pople, Gaussian 03, Revision B.01, Gaussian Inc., Pittsburgh, PA, 2003.
[14] R. Bauernschmitt, R. Ahlrichs, Chem. Phys. Lett. 256 (1996) 454.
[15] R.E. Stratmann, G.E. Scuseria, M.J. Frisch, J. Chem. Phys. 109 (1998) 8218.
[16] Y.A. Tobón, H.E. Di Loreto, C.O. Della Védova, R.M. Romano, J. Mol. Struct. 881 (2008) 139.
[17] L.C. Juncal, Y.A. Tobón, O.E. Piro, C.O. Della Védova, R.M. Romano, New J. Chem. 38 (2014) 3708.
[18] R.M. Romano, C.O. Della Védova, A.J. Downs, H. Oberhammer, S. Parsons, J. Am. Chem. Soc. 123 (2001) 12623.
[19] R.M. Romano, C.O. Della Védova, A.J. Downs, J. Phys. Chem. A 106 (2002) 7235.
[20] Y.A. Tobón, E.E. Castellano, O.E. Piro, C.O. Della Védova, R.M. Romano, J. Mol. Struct. 930 (2009) 43.
[21] B. Nelander, Chem. Phys. 159 (1992) 281.
[22] Y.A. Tobón, R.M. Romano, C.O. Della Védova, A.J. Downs, Inorg. Chem. 46 (2007) 4692.
[23] J.A. Gomez Castaño, A. Fantoni, R.M. Romano, J. Mol. Struct. 881 (2008) 68.
[24] R.M. Romano, A.J. Downs, J. Phys. Chem. A 107 (2003) 5298.
[25] R.M. Romano, A.L. Picone, A.J. Downs, J. Phys. Chem. A 110 (2006) 12129.
[26] V.I. Lang, J.S. Winn, J. Chem. Phys. 94 (1991) 5270.
[27] A.L. Picone, C.O. Della Védova, H. Willner, A.J. Downs, R.M. Romano, Phys. Chem. Chem. Phys. 12 (2010) 563.
[28] L. Schriver-Mazzuoli, A. Schriver, M. Wierzejewska-Hnat, Chem. Phys. 199 (1995) 227.